Ionic-Strength- and pH-Dependent Conformational States of Human Plasma Fibronectin†

Michael J. Benecky,* Richard W. Wine, Carl G. Kolvenbach,‡ and Michael W. Mosesson

Sinai Samaritan Medical Center, University of Wisconsin Medical School, Milwaukee Clinical Campus, Milwaukee, Wisconsin 53233

Received November 6, 1990; Revised Manuscript Received January 11, 1991

ABSTRACT: In order to provide a more detailed understanding of human plasma fibronectin (PFn) solution structure, we examined the effects of pH and ionic strength (μ) variation on the sedimentation velocities ($s_{20,w}$), fluorescence polarization-derived mean harmonic rotational relaxation times (ρ_H), far-ultraviolet (UV) circular dichroism (CD), and intrinsic tryptophan fluorescence of dimeric PFn and the monomeric 190/170-kDa PFn fragment. By comparing the biophysicial properties of PFn with those of the 190/170-kDa PFn fragment, we could assess the relative importance of intrasubunit and intersubunit electrostatic forces in the stabilization of PFn structure. The ρ_H derived from isothermal polarization measurements on 1-pyrenebutyrate conjugated PFn decreased markedly (4.5 → 1.05–1.23 μs) when μ was increased from 0.2 to 1.2 or when the pH was adjusted from 7.4 to 2.0 or 11.0. We also noted a significant decrease in the PFn $s_{20,w}$ (13 → 8.5–9.6S) under these same solvent conditions. In contrast, the ρ_H and $s_{20,w}$ of the monomeric 190/170-kDa PFn fragment were relatively insensitive to changes in μ or pH. Computer simulations of the observed pH-dependent changes in the far-UV CD of PFn and the 190/170-kDa PFn fragment revealed only minor differences in protein secondary structure. We also observed only small bathochromic shifts (1–3 nm) in the emission maxima of PFn and 190/170-kDa PFn fragment tryptophan fluorescence under acidic or high μ conditions. These results suggest that minimal changes in PFn tertiary (i.e., intrasubunit) structure occur at pH 2, 11, or at μ = 1.2. We therefore conclude that the driving force behind the observed pH- and μ-induced conformational changes in PFn is disruption of intersubunit electrostatic contacts. Our data suggest that the "unfolded" PFn conformation occurring at pH 2, 11, or μ = 1.2 can be approximated by a structure consisting of two independently rotating disk-shaped subunits, each having a diameter and thickness of 20 and 2.3 nm, respectively.

Human plasma fibronectin (PFn)[1] is a dimeric glycoprotein of molecular weight 520 000 (Sjöberg et al., 1987; Rocco et al., 1987) that mediates cell adhesion and migration in a wide variety of biological processes. Fibronectin-modulated cell-surface and cell–cell interactions probably play a significant role in wound healing, embryogenesis, phagocytosis, oncogenic transformation, and hemostasis. The adhesive biological activity of this molecule resides in its multiple binding affinities for various macromolecules found within cells, on cell surfaces, and in extracellular matrices.

Under physiological buffer conditions, PFn exhibits the hydrodynamic behavior predicted for a disk-shaped molecule with an approximate diameter and thickness of 30 and 2 nm, respectively (Sjöberg et al., 1987; Benecky et al., 1990). Structures observed during electron-microscopic examination of PFn specimens that had been deposited on carbon films and visualized by negative staining (Benecky et al., 1990) or STEM (Tooney et al., 1983) appear consistent with this model.

The $s_{20,w}$ of PFn decreases significantly under acidic, alkaline, and high ionic strength conditions (Alexander et al., 1979; Markovic et al., 1983). Laser light-scattering measurements revealed a marked decrease in the PFn diffusion constant at pH 11 (Williams et al., 1982). More recently, laser light scattering (Rocco et al., 1987) and small-angle X-ray scattering (Sjöberg et al., 1989) have shown that the PFn radius of gyration almost doubles in the presence of 1 M NaCl. All of these observations have been taken as evidence for a model in which the PFn molecule adopts an "extended" conformation under acidic, alkaline, and high ionic strength conditions. This extended conformation has been correlated with the appearance of PFn as a long slender strand (140 nm × 2 nm) during electron-microscopic examination of PFn samples that had been sprayed onto a mica surface in the presence of glycerol and visualized by platinum rotary shadowing (Erickson & Carrell, 1983).

The extended structures observed during electron-microscopic examination of rotary-shadowed PFn specimens are widely believed to represent the PFn solution structure under acidic, alkaline, or high ionic strength conditions [for example, see Erickson (1985) and Odermatt and Engel (1989)]. However, there are several observations that call into question

† This investigation was supported by NHLBI Program Project Grant HL-28444.

* Address correspondence to this author at the Sinai Samaritan Medical Center, Winter Research Institute, 950 North 12th Street, Milwaukee, WI 53201-0342.

‡ Present address: Amgen Corporation, 1900 Oak Terrace Lane, Thousand Oaks, CA 91320.

[1] Abbreviations: PFn, human plasma fibronectin; ρ_H, mean harmonic rotational relaxation time; TBS, Tris-buffered saline (50 mM Tris-HCl/150 mM NaCl, pH 7.4 buffer); EDTA, ethylenediaminetetraacetic acid; KIU, kallikrein inactivator units; PMSF, phenylmethanesulfonyl fluoride; SDS–PAGE, sodium dodecyl sulfate–polyacrylamide gel electrophoresis; PB-PFn, 1-pyrenebutyrate conjugated human plasma fibronectin; PB-190/170 kDa, 1-pyrenebutyrate conjugated 190/170-kDa fibronectin fragment; ρ_o, rotational relaxation time predicted for an equivalent hydrated sphere; η, solvent viscosity; μ, ionic strength; τ, fluorescence lifetime; $\langle\tau\rangle$, second-order average fluorescence lifetime; CD, circular dichroism; P, units of viscosity in poise; STEM, scanning transmission electron microscopy.

0006-2960/91/0430-4298$02.50/0

the validity of the correlation between the PFn solution structure at any given pH or ionic strength and the images of rotary-shadowed PFn observed in the electron microscope. Despite a previous report that glycerol induces a change in PFn conformation (Rocco et al., 1983), PFn samples are routinely exposed to high [≥30% (v/v)] glycerol concentrations during sample processing prior to rotary shadowing. Consistent with the occurrence of a glycerol-induced conformational change, we observed that rotary-shadowed PFn specimens that had been deposited on carbon in the presence of 30% glycerol yielded extended structures, whereas negatively-stained specimens that had been deposited on the same carbon substrate in the absence of glycerol yielded compact rounded structures (Benecky et al., 1990). These extended structures also appear difficult to reconcile with the observation that the dramatic change in PFn hydrodynamic behavior at pH 2 or 11 is accompanied by only a subtle change in its secondary structure (Alexander et al., 1979; Österlund, 1988). This model also appears inconsistent with recent fluorescence energy transfer measurements that indicate that the PFn intersubunit distance does not change in the presence of 1 M NaCl (Wolff & Lai, 1988, 1990).

In order to more precisely define the PFn conformational changes that occur under acidic, basic, and high ionic strength solution conditions, we investigated the effects of pH and ionic-strength variation on the sedimentation velocities, far-ultraviolet circular dichroism, intrinsic tryptophan fluorescence, and fluorescence polarization-derived mean harmonic rotational relaxation times of dimeric PFn and the monomeric 190/170-kDa PFn fragment. By comparing the biophysical properties of PFn with those of the 190/170-kDa PFn fragment, we were able to discern the relative importance of intrasubunit and intersubunit electrostatic forces in the stabilization of PFn structure. Our present data support PFn conformational changes in which acids, alkali, and high ionic strength selectively disrupt intersubunit electrostatic contacts while leaving the intrasubunit arrangement of salt bridges and/or hydrogen bonds largely intact.

Materials and Methods

Outdated human plasma was obtained from the Blood Center of Southeastern Wisconsin (Milwaukee, WI). We purchased succinimidyl-1-pyrenebutyrate [10% (w/w) adsorbed on Celite] from Molecular Probes (Eugene, OR). α-Thrombin was a generous gift from Dr. John Fenton (New York State Department of Health, Albany, NY). Sepharose 4B-CL, iodoacetamide, and Trasylol were from Pharmacia (Piscataway, NJ), Eastman Kodak (Rochester, NY), and Mobay Chemical Corporation (New York, NY), respectively. The gelatin–Sepharose 4B-CL affinity resin was prepared by a modification (Homandberg et al., 1985) of a previously reported method (March et al., 1974).

Isolation and Characterization of PFn and the Thrombin-Derived 190/170-kDa PFn Fragment. We isolated PFn from outdated human plasma employing gelatin–Sepharose 4B-CL chromatography with a 50 mM sodium citrate, 150 mM NaCl, pH 5.5 elution (Miekka et al., 1982; Smith & Griffin, 1985). PFn was quantified from its absorbance at 280 nm by using its known absorbance coefficient (ϵ = 1.28 cm^2 mg^{-1}) (Mosesson & Umfleet, 1970). PFn-containing fractions (>0.8 mg/mL) from the gelatin–Sepharose affinity resin were pooled, dialyzed against TBS, stored at 4 °C, and used within 2 weeks of isolation. During isolation and storage, all buffers and PFn stock solutions contained 0.5 mM EDTA, 0.10 mM PMSF, 0.02% (w/v) sodium azide, and 1 KIU/mL Trasylol. Upon SDS–PAGE (Laemmli, 1970) of reduced specimens on 5% polyacrylamide gels, PFn migrated as a closely spaced doublet at 220–225 kDa. SDS–PAGE under nonreducing conditions confirmed that >85% of the total protein migrated as the 450-kDa dimer with the remainder migrating in the position of the 235-kDa PFn component (Chen et al., 1977). In experiments designed to test the possibility of PFn interchain disulfide-bond exchange, protein samples (0.5 mg/mL) were dialyzed overnight against a deoxygenated 50 mM sodium bicarbonate, 150 mM NaCl, pH 9.0 buffer in the presence and absence of 10 mM iodoacetamide. For the entire reaction period, anaerobic conditions were maintained by bubbling nitrogen gas through the dialysis buffers. The respective amounts of covalently linked PFn dimer in these samples were estimated by SDS–PAGE on 4% polyacrylamide gels under nonreducing conditions.

The 190/170-kDa PFn fragment was isolated from a thrombin digest of PFn by gelatin-Sepharose 4B-CL chromatography with a 3 M urea–TBS elution (Homandberg & Erickson, 1986; Benecky et al., 1988). We quantified this fragment from its absorbance at 280 nm using ϵ = 1.20 cm^2 mg^{-1} (Homandberg & Erickson, 1986). Size heterogeneity of the 190/170-kDa PFn fragment reflected the slightly different lengths of the "A" and "B" PFn subunits (Click & Balian, 1985). The amino acid sequence of this peptide begins at position 260 (Homandberg & Erickson, 1986) in the PFn sequence (Kornblihtt et al., 1985). Therefore, this fragment lacks the 30-kDa amino-terminal domain. We have previously shown that this large monomeric PFn fragment retains all of the gelatin- and heparin-binding activity exhibited by the native dimeric molecule (Benecky et al., 1988, 1990).

Preparation and Characterization of the 1-Pyrenebutyrate Conjugates of PFn and the 190/170-kDa PFn Fragment. The 1-pyrenebutyrate conjugates of PFn and the 190/170-kDa PFn fragment were prepared by the use of the amine-reactive reagent succinimidyl-1-pyrenebutyrate (Benecky et al., 1990). Gelatin–Sepharose 4B-CL affinity chromatography was employed to separate PB-PFn and PB-190/170 kDa from unreacted succinimidyl-1-pyrenebutyrate (Benecky et al., 1990). We have previously shown that the labeling reaction with 1-pyrenebutyrate is not confined to any specific region on the PFn subunit (Benecky et al., 1990). The number of dye molecules bound per protein molecule was determined by absorption spectroscopy using a molar extinction coefficient of 4.0 × 10^4 M^{-1} cm^{-1} at 346 nm for protein-bound 1-pyrenebutyrate (Knopp & Weber, 1969). The protein conjugates employed in this study contained 0.3–0.8 mol of 1-pyrenebutyrate per mole of protein. Under these conditions, PB-PFn and PB-190/170 kDa retained all the gelatin- and heparin-binding activity present in native PFn (Benecky et al., 1990). This degree of labeling had no discernible effect on the $s_{20,w}$ and far-UV CD spectra of PFn and the 190/170-kDa PFn fragment (Benecky et al., 1990).

Relative Fluorescence Quantum Yield Measurements. Fluorescence data were obtained on a SLM-Aminco SPF500C spectrofluorometer equipped with the manufacturer's polarization accessory. The reported emission spectra were excited at 330 nm with both excitation and emission polarizers in the vertical position. Slit widths for the excitation and emission ports were adjusted to yield a 7.5-nm band-pass. These spectra were corrected for the solvent background but were left uncorrected for the wavelength-dependent response of the photomultiplier. The relative quantum yields of PB-PFn and PB-190/170-kDa fluorescence were estimated by integrating their respective emission spectra in the 350–450 nm interval. The protein sample concentrations were at 0.2 mg/mL. We

examined the effects of pH by employing a set of $\mu = 0.2$ buffers with pH values of 2.0, 7.4, and 11.0, respectively (Miller & Golder, 1950). For these experiments, we utilized the following buffers: 5.3 mM glycine-HCl and 185 mM NaCl, pH 2; 8.6 mM sodium phosphate and 180 mM NaCl, pH 7.4; and 7.6 mM glycine-NaOH and 188 mM NaCl, pH 11. To examine the effects of high ionic strength, we employed the 8.6 mM sodium phosphate and 1.18 M NaCl, pH 7.4 buffer. Unless stated otherwise, these buffers were employed throughout this study.

Variable-Frequency Phase-Modulation Fluorescence Lifetime Measurements. We measured the PB-PFn fluorescence lifetime using the phase-modulation technique (Lakowicz, 1983a). These measurements were made on a SLM 48000S multiple-frequency phase-modulation spectrofluorometer at SLM Instruments, Inc., Urbana, IL. Glycogen was used as the zero lifetime standard. The exciting light ($\lambda_{ex} = 330$ nm) passed through a 2-nm band-pass slit, and we utilized an optical cutoff filter to collect all fluorescence having $\lambda_{em} > 370$ nm. The concentrations of PB-PFn samples were 1 mg/mL. Sample temperature was maintained at 20.0 ± 0.10 °C with a jacketed cell holder and a circulating water bath. For each given pH and ionic strength studied, we measured the phase-shift and demodulation of PB-PFn fluorescence as a function of modulation frequency between 0.8 and 3.0 MHz. We calculated the fluorescence lifetime(s) of PB-PFn from these data using an analysis previously outlined by Weber (1981). We performed these computations on an IBM PS/2 computer utilizing the software package that accompanied the SLM 48000S spectrofluorometer. In the case of double-exponential fluorescence decay, we employed the second-order average lifetime, $\langle\tau\rangle = (\alpha_1^2\tau_1^2 + \alpha_2^2\tau_2^2)/(\alpha_1\tau_1 + \alpha_2\tau_2)$, in subsequent ρ_H calculations (Brochon & Wahl, 1972). In this equation, α and τ denote the fractional contribution and fluorescence lifetime of the first (subscript 1) and second (subscript 2) decay component, respectively.

Fluorescence Polarization Measurements. We measured the fluorescence polarization, P, exhibited by the 1-pyrenebutyrate conjugates of PFn and the 190/170-kDa PFn fragment using the single-channel method (Lakowicz, 1983b):

$$P = \frac{(I_{VV} - B_{VV}) - G(I_{VH} - B_{VH})}{(I_{VV} - B_{VV}) + G(I_{VH} - B_{VH})} \quad (1)$$

where $G = I_{HV}/I_{HH}$. I is the observed fluorescence intensity when the excitation (first subscript) and emission (second subscript) polarizers were in the vertical (V) and horizontal (H) positions, respectively. B is the emission intensity of a blank containing the same amount of underivatized PFn or 190/170-kDa PFn fragment under the identical experimental conditions. G is an instrument correction factor that accounts for the differences in the transmission efficiency of the optical path for vertically and horizontally polarized light. For these measurements, the excitation and emission wavelengths were set to 330 and 398 nm, respectively. The excitation and emission slits were both adjusted to yield a 7.5-nm band-pass. The concentration of protein samples was approximately 0.2 mg/mL. Each fluorescence-intensity determination was performed at 20.0 ± 0.1 °C on duplicate samples, with a single measurement representing an average of 160 independent readings. The resulting polarization values were reproducible to within ±0.001.

Analysis of the Fluorescence Polarization Data with the Perrin Equation. If rapid localized rotational motion of the fluorescent probe makes a contribution to the observed depolarization that is independent of the depolarization arising from the slow overall rotational motion of the protein, the depolarization associated with the overall rotation of PB-PFn or PB-190/170-kDa molecules is expected to obey the following linear relationship (Wahl & Weber, 1967; Weltman & Edelman, 1967):

$$1/P - 1/3 = (1/P_1 - 1/3)[1 + \beta(T/\eta)] \quad (2)$$

where $1/P_1 - 1/3 = (1/[1 - f(T)])(1/P_0 - 1/3)$ and $\beta = R\tau/V$. Therefore, a plot of $(1/P - 1/3)$ vs the temperature to solvent viscosity ratio (T/η) yields a line with a slope of $\beta(1/P_1 - 1/3)$ and an intercept of $1/P_1 - 1/3$. β is a parameter determined from the ratio of the slope to the intercept of the Perrin plot, R is the gas constant, τ is the fluorescence lifetime, and V is the molecular volume. The fraction of the total fluorescence intensity arising from the rapidly rotating fluorescent probe, $f(T)$, increases in its relative proportion at higher sample temperatures. P_0 is the observed polarization in the absence of all molecular rotational motion (i.e., $T/\eta = 0$). P_1 corresponds to the polarization where the overall rotational motion of the protein molecule is frozen, while the protein side chains bearing the fluorescent probe continue to rotate freely. The term $1/P_1 - 1/3$, which is derived from an experiment in which solvent viscosity was varied by the addition of sucrose at constant temperature (i.e., conditions where $f(T)$ is constant), will be larger than $1/P_0 - 1/3$ when depolarization due to localized probe rotation is operative. We can then calculate the rotational relaxation time, ρ, provided τ is known:

$$\rho = (3\tau/\beta)(T/\eta)^{-1} \quad (3)$$

In all of our subsequent rotational relaxation time calculations, we assumed the solvent to be water at 25 °C ($T/\eta = 3.34 \times 10^4$ K P^{-1}). Eq 3 can only be applied rigorously to spherical molecules (Perrin, 1934). However, Weber (1953) has extended this treatment to include elliptical macromolecules. In this case, the measured rotational relaxation time corresponds to ρ_H, the harmonic mean of the rotational relaxation times about the principal axes of the ellipsoid. Eq 1 indicates that ρ_H can be determined from the linear low-viscosity component (i.e., ≤30% sucrose at 20 °C; $T/\eta > 8000$ K P^{-1}) of the isothermal Perrin plot, since this depolarization is derived exclusively from the slow overall rotation of the protein molecule. Downward curvature in the isothermal Perrin plot at high viscosity (i.e., ≥40% sucrose at 20 °C; $T/\eta < 5000$ K P^{-1}) originates from the rapid localized rotational motion of the protein side chains bearing the fluorescent probe (Benecky et al., 1990).

Perrin plots were constructed from polarization data obtained as a function of sucrose concentration [0–30% (w/v)] at constant temperature (20 °C). These analyses utilized previously tabulated sucrose viscosity data (Sober, 1970). At $\mu = 0.2$, we ignored the small increment in viscosity contributed by the buffer components. However, the additional solvent viscosity contributed by 1.18 M NaCl proved to be significant in PB-PFn samples having sucrose concentrations of less than 10% (w/v). Therefore, we narrowed our experimental range of viscosities to between 10 and 30% (w/v) sucrose for PB-PFn at $\mu = 1.20$. P_0 was estimated from the intercept of a Perrin plot constructed from polarization data obtained as a function of temperature (Benecky et al., 1990).

Rotational Relaxation Times Expected for Various Hydrodynamic Models. (A) Sphere. The rotational relaxation time, ρ_o, expected if PFn were a hydrated rigid sphere, was estimated by

$$\rho_o = 3\eta V/RT \quad (4)$$

Substituting $R = 8.314 \times 10^7$ erg mol^{-1} K^{-1}, $T = 298$ K, $\eta = 0.0089$ P, and $V = 5.82 \times 10^5$ cm^3 mol^{-1} into this equation, we obtained $\rho_0 = 6.28 \times 10^{-7}$ s. This calculation assumed that PFn had a molecular weight of 520 000, a partial specific volume of 0.72 mL/g (Mosesson et al., 1975), and a hydration of 0.4 g of H_2O/g of protein (Rocco et al., 1987). Using an average molecular weight of 180 000 and making similar assumptions for partial specfici volume and hydration, we estimated $\rho_0 = 2.17 \times 10^{-7}$ s for the thrombin-derived 190/170-kDa PFn fragment.

(B) Elliptical Models. We have previously described the derivation of functions relating the ρ_H/ρ_0 ratio to ellipticity (Benecky et al., 1990). These functions were used to calculate the mean harmonic rotational relaxation times expected for various prolate (i.e., cigar-shaped) and oblate (i.e., disk-shaped) ellipsoidal structures (Benecky et al., 1990).

Intrinsic Protein Tryptophan Fluorescence Measurements. For these measurements, the polarization accessory was removed from the SLM SPF500C spectrofluorometer. The reported emission spectra employed 295-nm excitation and slits for the excitation and emission ports were both adjusted to yield a 4-nm band-pass. These spectra were corrected for the solvent background but were left uncorrected for the wavelength-dependent response of the photomultiplier. Native underivatized protein samples were at a concentration of 15 μg/mL.

Analytical Ultracentrifugation. Sedimentation velocity measurements were made at 20 °C in a Beckman Model E analytical ultracentrifuge equipped with a photoelectric UV scanner. Centrifugation runs were at 56 000 rpm. For these experiments, protein concentrations were at 0.7 mg/mL.

Far-Ultraviolet Circular-Dichroism Measurements. CD spectra were recorded on a Jasco J500A spectropolarimeter that had been interfaced to an IBM-compatible computer. In order to investigate the effects of acidic and alkaline conditions on the far-UV CD spectra of PFn and the 190/170-kDa PFn fragment, protein samples (0.5 mg/mL) were dialyzed against the following buffers: 50 mM sodium phosphate, pH 2; 50 mM sodium phosphate, pH 7.4; and 50 mM sodium phosphate, pH 11. Protein concentration measurements employed $\epsilon = 1.28$ cm^2 mg^{-1} for the 280-nm absorbance coefficient at each pH we studied. Samples subjected to CD analysis were transferred to 0.2-mm path-length cylindrical quartz cells. We signal-averaged four scans, each of which consisted of 251 equally spaced data points in the 240–190-nm interval. We employed a scan speed of 5 nm/min, a gain of 10 mdeg/full scale and a 4-s time constant. The solvent background obtained under the identical experimental conditions was subtracted from the raw CD data. Conversion of the CD data to mean residue ellipticity assumed a mean residue molecular weight of 108 (Österlund et al., 1985). From these data, we estimated the protein secondary-structure distribution using CONTIN software (Provencher & Glöckner, 1981) on a Digital Equipment Corporation VAX computer at Marquette University (Milwaukee, WI).

Results

pH- and Ionic-Strength-Dependent Changes in the Lifetime and Relative Intensity of PB-PFn Fluorescence. Characterization of the pH and ionic-strength dependence of the PB-PFn fluorescence lifetime were prerequisites to the use of steady-state fluorescence polarization as a probe of PFn structure under acidic, alkaline, and high ionic strength solution conditions (Figure 1A, Table I). We also monitored the relative intensity of PB-PFn fluorescence as a function of pH (Figure 1B) and ionic strength (data not shown), because changes in this parameter often mirror changes in τ (Lakowicz, 1983c). The relative intensity of PB-PFn fluorescence did not change when the ionic strength was increased from 0.2 to 1.2 at pH 7.4 (data not shown). Consistent with this observation, the second-order average fluorescence lifetimes ($\langle\tau\rangle$) calculated from the $\mu = 0.2$ and $\mu = 1.2$ PB-PFn variable-frequency phase-modulation data were identical (123 ns; Table I). Relative to the values obtained at pH 7.4, modest increases (4–7%) in both average fluorescence lifetime and relative fluorescence intensity were observed under acidic conditions (i.e., pH 2 and $\mu = 0.2$). Under alkaline conditions (i.e., pH 11 and $\mu = 0.2$), the average lifetime and the relative intensity of PB-PFn fluorescence decreased by 15% and 30%, respectively. The relative intensities of PB-PFn and PB-190/170-kDa fluorescence were identical at each pH and ionic strength investigated in this study (data not shown). This validated our assumption in the subsequent analysis of the PB-190/170-kDa fluorescence-polarization data that PB-190/170 kDa displayed the same fluorescence lifetime as did PB-PFn.

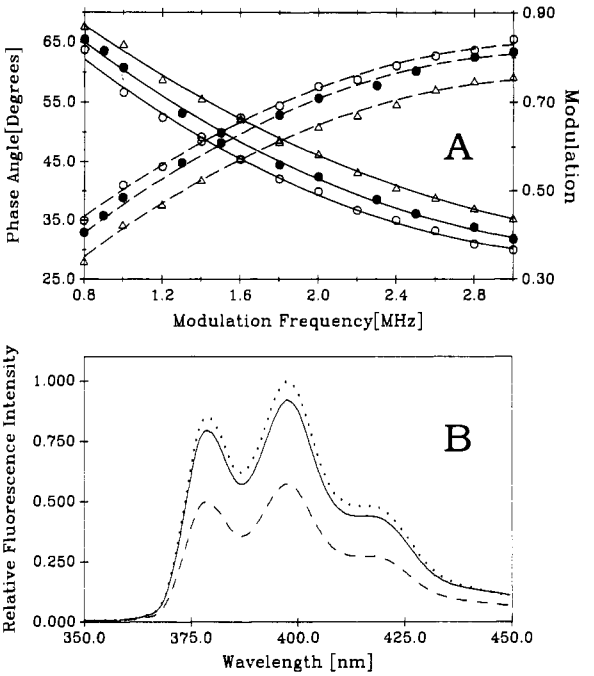

FIGURE 1: (A) Phase (solid lines) and modulation (dashed lines) data used to determine the effect of pH variation on the PB-PFn fluorescence lifetime: (●—●) pH 7.4 phase angle data; (●---●) pH 7.4 modulation data; (○—○) pH 2.0 phase angle data; (○---○) pH 2.0 modulation data; (△—△) pH 11 phase angle data; and (△---△) pH 11 modulation data. Symbols denote the experimental data, while the dashed or solid lines display the theoretical fits to models assuming doubly exponential fluorescence decay. Fluorescence decay parameters derived from these measurements are summarized in Table I. (B) Changes in the relative intensity of PB-PFn fluorescence observed in $\mu = 0.2$ buffers having pH values of 2.0 (dotted line), 7.4 (solid line), and 11.0 (dashed line), respectively.

Table I: pH- and Ionic-Strength-Dependent Variation in the Parameters of PB-PFn Fluorescence Decay Derived from Variable-Frequency Phase-Modulation Measurements[a]

solvent condns[b]	α_1	τ_1 (ns)	α_2	τ_2 (ns)	$\langle\tau\rangle$ (ns)[c]
pH 7.4; $\mu = 0.2$	0.0652	33.6	0.9348	134.0	123.2
pH 7.4; $\mu = 1.2$	0.0818	37.2	0.9182	137.4	123.3
pH 11; $\mu = 0.2$	0.0611	14.6	0.9389	114.7	106.8
pH 2.0; $\mu = 0.2$	0.1400	57.7	0.8600	157.5	128.3

[a] All analyses assumed doubly exponential fluorescence decay with α and τ denoting each component's fractional contribution and fluorescence lifetime, respectively. [b] Buffers are described under Materials and Methods. [c] Computation of the second-order average fluorescence lifetime assumed $\langle\tau\rangle = (\alpha_1^2\tau_1^2 + \alpha_2^2\tau_2^2)/(\alpha_1\tau_1 + \alpha_2\tau_2)$.

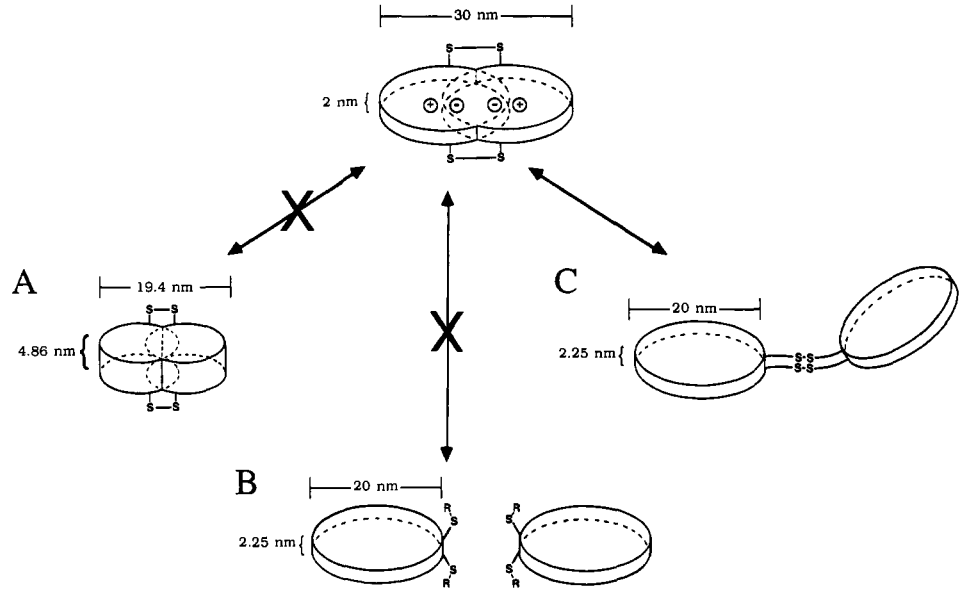

Scheme I: Structural models for the "unfolded PFn conformation" supported by the observation of a significantly shorter PFn ρ_H value (1.05–1.23 μs) under acidic, alkaline, or high ionic strength conditions. (A) In model A, the axial ratio of the disk-shaped (oblate) PFn molecule decreases from a value of 15:1 under physiological buffer conditions to 4:1 at pH 2, at pH 11, or in the presence of 1.2 M NaCl at pH 7.4. (B) Model B assumes that there is an equilibrium between dimeric and monomeric PFn forms, which strongly favors covalently linked PFn dimer formation under physiological buffer conditions. We postulate that the salt- or pH-induced disruption of intersubunit electrostatic contacts shifts this equilibrium to favor PFn monomer formation under acidic, alkaline, or high ionic strength solution conditions. Note that rearrangement of the PFn intersubunit disulfide bonds is an implicit feature of this model. (C) In model C, changes in pH or ionic strength induce an unfolded structure consisting of two loosely associated disk-shaped subunits. This structure permits the independent rotational motion of each PFn subunit about the carboxyl-terminal interchain disulfide bonds. This conformational change is presumably mediated by the salt- or pH-induced disruption of intersubunit salt bridges and/or hydrogen bonds.

Table II: Effect of pH and Ionic Strength on the Sedimentation Rates of PFn and the 190/170-kDa PFn Fragment

solvent condns	$s_{20,w}$[a]
PFn	
pH 7.4; μ = 0.2	13.0
pH 7.4; μ = 1.2	9.6
pH 11.0; μ = 0.2	8.5
pH 2.0; μ = 0.2	8.6
190/170-kDa PFn Fragment	
pH 7.4; μ = 0.2	6.1
pH 7.4; μ = 1.2	5.5
pH 11.0; μ = 0.2	5.6
pH 2.0; μ = 0.2	6.2

[a] Average experimental uncertainty was ±0.3 S.

Effect of High Ionic Strength on the Hydrodynamic Properties of PFn and the 190/170-kDa PFn Fragment. Two mutually independent processes give rise to the depolarization exhibited by the 1-pyrenebutyrate conjugates of PFn and the 190/170-kDa PFn fragment: (a) rapid (subnanosecond) "thermally activated" rotational motion of the protein side chains bearing the fluorescent probe (Weber, 1952) and (b) slow (microsecond) temperature-independent global rotational motion of the entire protein molecule (Benecky et al., 1990). Only the rotational relaxation time associated with the latter process is a hydrodynamic parameter that can be used to probe protein structure. Perrin plots constructed from polarization measurements made as a function of temperature yield anomalously short ρ_H values when thermally activated probe rotation is present (Wahl & Weber, 1967; Weltman & Edelman, 1967; Rawitch et al., 1969; Acuña et al., 1987; Benecky et al., 1990). Probe rotation also gives rise to nonlinearity in the high-viscosity region [$T/\eta < 8000$ K P^{-1}; i.e., >35% (w/v) sucrose at 20 °C] of the isothermal Perrin plot (Wahl & Weber, 1967; Benecky et al., 1990). We therefore discriminated against the thermally activated depolarization

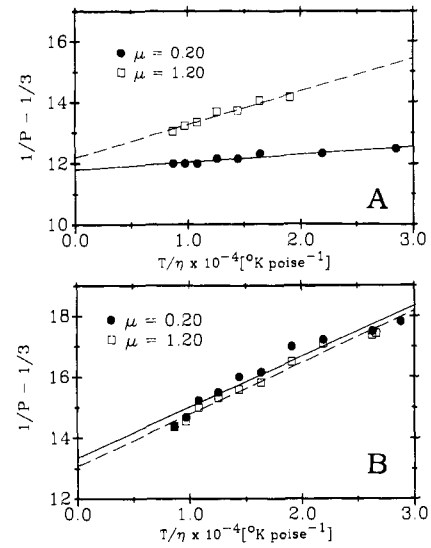

FIGURE 2: Perrin plots constructed from experiments in which (A) PB-PFn or (B) PB-190/170-kDa fluorescence polarization was monitored while solvent viscosity was varied by the addition of sucrose to pH 7.4 buffers having ionic strengths of 0.2 (●—●) and 1.2 (○---○), respectively, at a constant temperature (20 °C).

arising from probe rotation in our present experimental system by employing low sucrose concentrations [0–30% (w/v)] at a constant temperature (20 °C). Under these conditions, all of the observed depolarization emanates from the slow global rotational motion of the protein molecule (Benecky et al., 1990). The ρ_H (4.5 ± 1.0 μs) calculated from the μ = 0.2 PB-PFn isothermal polarization data (Figure 2A, circles) was indistinguishable from the value we previously obtained in PBS (4.4 ± 0.9 μs; Benecky et al., 1990). However, the Perrin plot constructed from the μ = 1.2 polarization data (Figure 2A, squares) yielded a significantly shorter ρ_H (1.23 ± 0.18 μs). Concomitantly, we also noted a sharp (26%) decrease in the

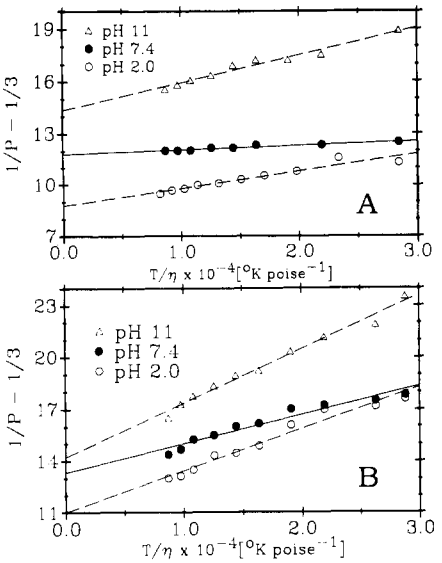

FIGURE 3: Perrin plots constructed from experiments in which (A) PB-PFn or (B) PB-190/170-kDa fluorescence polarization was monitored while solvent viscosity was varied by the addition of sucrose to $\mu = 0.2$ buffers having pH values of 2.0 (○), 7.4 (●) and 11.0 (△), respectively, at a constant temperature (20 °C).

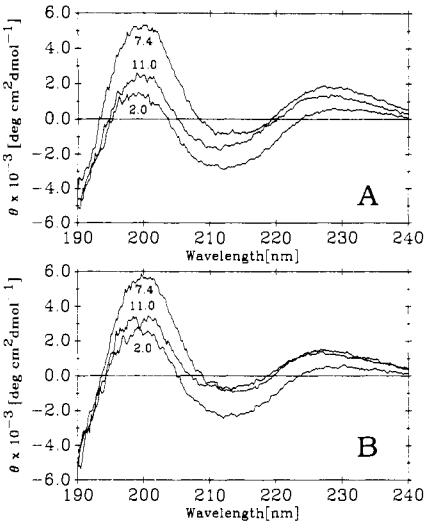

FIGURE 4: Far-ultraviolet CD spectra of (A) PFn or (B) the 190/170-kDa PFn fragment obtained in 50 mM sodium phosphate buffers having pH values of 2.0 (bottom trace), 7.4 (top trace), and 11.0 (middle trace), respectively. The method of Provencher and Glöckner (1981) was used to estimate changes in protein secondary structure distribution from these data. These results are summarized in Table III.

PFn $s_{20,w}$ when the ionic strength was increased from 0.2 to 1.2 (Table II). The observed changes in ρ_H and $s_{20,w}$ at μ = 1.2 could be reversed by sample dialysis against a $\mu = 0.20$ buffer (data not shown). Taken by itself, the observation of a significantly shorter ρ_H under high ionic strength conditions suggested at least three possible models (illustrated in Scheme I) for the high ionic strength induced PFn conformational change.

In order to determine whether perturbation of the three-dimensional arrangement of salt bridges/hydrogen bonds within a PFn subunit occurred under high ionic strength conditions, we studied the ionic strength dependence of the 190/170-kDa PFn fragment ρ_H (Figure 2B) and $s_{20,w}$ (Table II). These studies were motivated by our previous finding that the thrombin-derived 190/170-kDa PFn fragment retains the secondary and tertiary structure (i.e., intrasubunit properties) of the native PFn dimer but due to its monomeric nature is devoid of quaternary (i.e., intersubunit) structure (Benecky et al., 1990). In contrast to the PB-PFn result (Figure 2A), the rotational relaxation times calculated from the $\mu = 0.2$ and $\mu = 1.2$ PB-190/170 kDa isothermal polarization data were identical (0.93 ± 0.09 μs). Comparison of the $s_{20,w}$ values of the 190/170-kDa PFn fragment obtained at $\mu = 0.2$ and $\mu = 1.2$, respectively, did not reveal any significant difference (6.1 ± 0.3S vs 5.5 ± 0.3S).

To test the possibility of PFn intersubunit disulfide-bond exchange implicated in model B (Scheme I), we attempted to "trap" the postulated noncovalently linked dimeric PFn intermediates of this exchange process using iodoacetamide. However, as monitored by SDS–PAGE under nonreducing condtions, identical amounts of covalently linked PFn dimer (450 kDa) were found in PFn samples that had been subjected to anaerobic dialysis in the presence and absence of 10 mM iodoacetamide (data not shown).

pH-Induced Changes in the Hydrodynamic Properties of PFn and the 190/170-kDa PFn Fragment. The ρ_H of PB-PFn decreased from 4.5 ± 1.0 μs at pH 7.4 to 1.05 ± 0.10 μs and 1.07 ± 0.10 μs at pH 2 and pH 11, respectively (Figure 3A). Confirming previously published work (Alexander et al., 1979; Markovic et al., 1983), we also observed a marked decrease in the PFn sedimentation rate under acidic or alkaline conditions (Table II). To assess the sensitivity of PFn intrasubunit electrostatic interactions to acid and alkali exposure, we examined the effect of pH variation on the ρ_H (Figure 3B) and $s_{20,w}$ (Table II) of the monomeric 190/170-kDa PFn fragment. Analogous to the situation at $\mu = 1.2$ (Table II), examination of the pH dependence of the 190/170-kDa PFn fragment sedimentation rate revealed small differences that were within the experimental uncertainty of this type of measurement (±0.3 S). However, the ρ_H of PB-190/170 kDa decreased from 0.93 ± 0.09 μs at pH 7.4 to 0.62 ± 0.06 μs and 0.45 ± 0.05 μs at pH 2 and pH 11, respectively (Figure 3B). We note, however, that the magnitude of these pH-dependent effects are relatively smaller than those observed for the dimeric PB-PFn molecule (Figure 3A).

Table III: pH-Dependent Changes in PFn and 190/170-kDa PFn Fragment Secondary-Structure Distribution Estimated from the Far-Ultraviolet CD Spectral Data

pH[a]	n[b]	α-helix (%)	β-sheet (%)	remainder (%)[c]
		PFn		
7.4	22	0	83 ± 5	17 ± 5
2.0	7	2 ± 3	74 ± 6	24 ± 7
11.0	8	2 ± 3	81 ± 1	17 ± 4
		190/170 kDa PFn Fragment		
7.4	6	1 ± 2	79 ± 4	20 ± 4
2.0	3	4 ± 1	77 ± 1	19 ± 1
11.0	5	0	74 ± 7	26 ± 7

[a] 50 mM sodium phosphate buffers were employed. [b] The number of independent experiments that were averaged. [c] Aperiodic secondary-structure elements (e.g., random coil, β-turn) were grouped in the "remainder" class.

pH-Induced Changes in the Far-Ultraviolet Circular Dichroism of PFn and the 190/170-kDa PFn Fragment. Observation of pH-dependent changes in the ρ_H of the monomeric PB-190/170-kDa derivative (Figure 3B) suggested that some perturbation of intrasubunit salt bridges had also occurred under acidic or alkaline conditions. Since it appeared likely that changes in PFn secondary structure would accompany the pH-dependent rearrangement of its intrasubunit salt bridges, we studied the effects of these solvent conditions on the far-UV CD spectra of PFn (Figure 4A) and the 190/170-kDa PFn fragment (Figure 4B). Although pH-dependent

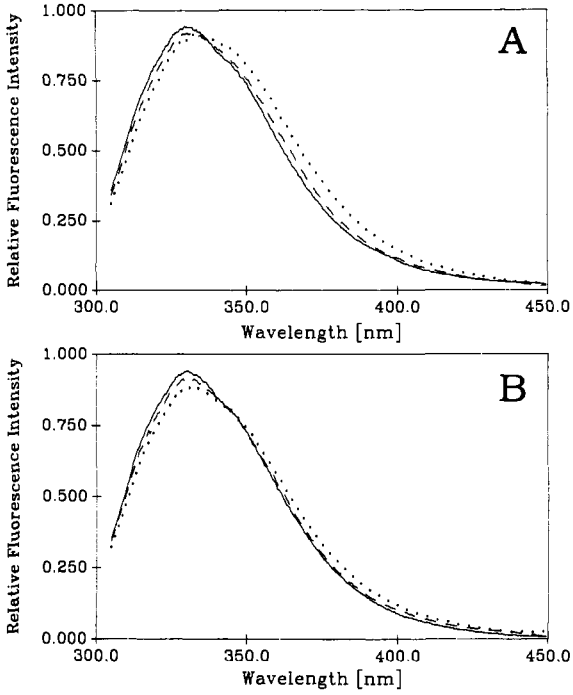

FIGURE 5: Intrinsic tryptophan fluorescence exhibited by (A) PFn or (B) the 190/170-kDa PFn fragment at $\mu = 0.2$ and pH 7.4 (solid line), at $\mu = 1.2$ and pH 7.4 (dashed line), and at $\mu = 0.2$ and pH 2.0 (dotted line).

CD spectral changes were observed for both PFn and the 190/170-kDa PFn fragment (Figure 4), computer simulations of these spectral changes suggested that only minor changes in the distribution of secondary structure occurred within PFn and 190/170-kDa PFn fragment molecules at pH 2 or pH 11 (Table III). The observation of an acid-induced change in the PFn far-UV CD spectrum confirmed a previously published result (Österlund, 1988).

Changes in the Intrinsic Tryptophan Fluorescence of PFn and the 190/170-kDa PFn Fragment Observed Under Acidic and High Ionic Strength Conditions. In order to better understand the nature of the PFn conformational change that had occurred under acidic or high ionic strength conditions, we characterized the effects of these conditions on the intrinsic tryptophan fluorescence (i.e., $\lambda_{ex} = 295$ nm) of PFn (Figure 5A) and the 190/170-kDa PFn fragment (Figure 5B). This technique, which utilizes the exquisite sensitivity of tryptophan fluorescence to changes in the solvent polarity of their microenvironments within a protein, has been used extensively to monitor subtle changes in protein conformation (Lakowicz, 1983c). In a $\mu = 0.2$ buffer at pH 7.4, both PFn and the 190/170-kDa PFn fragment exhibited emission maxima at 330 nm. This value shifted to 331 and 333 nm at $\mu = 1.2$ and pH 2, respectively. Interference from tyrosinate fluorescence (e.g., *N*-acetyltryosinamide exhibited $\lambda_{ex} = 292$ nm and $\lambda_{em} = 407$ at pH 11) precluded the application of this technique at pH 11.

Discussion

PFn Structure under High Ionic Strength Conditions. In this investigation, we observed that the rotational relaxation time associated with the global rotational motion of the dimeric PFn molecule decreased markedly (4.5 μs → 1.23 μs; Figure 2A) under high ionic strength conditions. Taken by itself, this result appeared consistent with three possible models for the ionic-strength-induced PFn conformational change (Scheme I). PFn structures consistent with model A (i.e., $\rho_H/\rho_o = 2$) include an oblate (disk-shaped) ellipsoid with a 4:1 axial ratio or a prolate (cigar-shaped) ellipsoid with an axial ratio greater than 10:1 [see Figure 6 in Benecky et al. (1990)]. Both of these shapes would display lower translational frictional resistance (i.e., faster sedimentation velocities) than native PFn (an oblate ellipsoid with a 15:1 axial ratio) does under physiological buffer conditions (Cantor & Schimmel, 1980). Consequently, the observation of a reduced PFn sedimentation rate under high ionic strength conditions (Alexander et al., 1979; Markovic et al., 1983; Table II) excludes model A from further consideration.

If our assumption that the driving force behind both models B and C is the salt-induced disruption of intersubunit electrostatic contacts is correct, one would also expect the three-dimensional intrasubunit arrangement of PFn domains to be relatively insensitive to ionic strength changes. In apparent agreement with these predictions, we observed that the ρ_H (Figure 2B), $s_{20,w}$ (Table II), and intrinsic tryptophan emission (Figure 5B) of the monomeric 190/170-kDa PFn fragment were all largely insensitive to ionic-strength changes. In contrast, dramatic ionic-strength-dependent changes in the $s_{20,w}$ (Table II) and ρ_H (Figure 2A) of the dimeric PFn molecule were observed. Since rearrangement of PFn's interchain disulfide bonds is an implicit feature of model B, we employed iodoacetamide in an attempt to trap the putative noncovalently linked dimeric PFn intermediates of this exchange reaction. However, as assessed by SDS–PAGE under nonreducing conditions, identical amounts of the covalently linked PFn dimer were found in samples that had been subjected to anaerobic dialysis in the presence and absence of iodoacetamide. On the basis of this observation, model B was excluded from further consideration. We must therefore conclude that model C is the most likely model for the ionic-strength-induced PFn conformational change.

The ρ_H of PB-PFn (1.23 μs) calculated from the $\mu = 1.2$ polarization data (Figure 2A) is approximately 4 times longer than that predicted for a rigid hydrated sphere of molecular weight 260 000. This finding supports a model in which the high ionic strength "unfolded" conformation of PFn can be approximated by a structure consisting of two independently rotating disk-shaped subunits (each having an approximate axial ratio of 9:1) that remain covalently linked to one another through a pair of carboxyl-terminal interchain disulfide bonds (Petersen et al., 1983). Assuming a partial specific volume of 0.72 mL/g (Mosesson et al., 1975) and a hydration of 0.4 g of H_2O/g of protein (Rocco et al., 1987), we calculate that each isolated PFn subunit would have a diameter and thickness of 20.0 and 2.3 nm, respectively. Since we can not exclude the possibility that the intersubunit disulfide bonds partially restrict PFn subunit rotational motion, our present analysis may overestimate the spherical asymmetry of each PFn subunit. We have previously estimated the diameter and thickness of the whole PFn molecule to be 30 and 2 nm, respectively under physiological buffer conditions (Benecky et al., 1990).

PFn Structure at pH 2 or 11. The ρ_H or PB-PFn decreased from a value of 4.5 μs at pH 7.4 to 1.1 μs at pH 2 or pH 11, respectively (Figure 3A). We also observed a concomitant decrease in PFn sedimentation velocity under these solvent conditions (Table II). We again interpret these observations as being indicative of an unfolded structure that permits the independent rotational motion of each PFn subunit (i.e., model C). Analogous to the situation at high ionic strength, this model predicts that the electrostatic contacts between PFn subunits would be especially sensitive to acid or alkali exposure. Furthermore, there is no need to invoke any pH-dependent change in the three-dimensional arrangement of salt bridges

and/or hydrogen bonds within an isolated PFn subunit. Experimental observations that appear consistent with these predictions include (1) the relative insensitivity of the $s_{20,w}$ of the monomeric 190/170-kDa PFn fragment to changes in pH (Table II) and (2) the analyses (Table III) of the PFn far-ultraviolet CD spectral data (Figure 4A), which indicate that only minor changes in the distribution of PFn secondary structure accompany the dramatic pH-induced changes in its ρ_H (Figure 3A) and sedimentation velocity (Table II).

Evidence that PFn Tertiary (Intrasubunit) Structure Remains Largely Unaffected by Changes in Solution pH and Ionic Strength. The ρ_H of the monomeric PFn derivative, PB-190/170 kDa, decreased from a value of 0.93 μs at pH 7.4 to 0.62 and 0.45 μs at pH 2 and 11, respectively (Figure 3B). This observation raised the possibility that significant disruption of intrasubunit salt bridges and/or hydrogen bonds also had occurred under acidic or alkaline conditions. In order to assess the extent of PFn intrasubunit structural rearrangement, we examined the effects of pH variation on the $s_{20,w}$, intrinsic tryptophan fluorescence, and far-ultraviolet circular dichroism of the monomeric 190/170-kDa PFn fragment. The $s_{20,w}$ of the 190/170-kDa PFn fragment did not change significantly under acidic or alkaline conditions (Table II). Analyses of the pH dependence of the 190/170-kDa PFn fragment CD data revealed only minor differences in protein secondary-structure distribution (Table III). In addition, we observed only a modest bathochromic shift (330 → 333 nm) in the emission maxima of PFn and 190/170-kDa PFn fragment tryptophan fluorescence under acidic conditions (Figure 5). From these observations, we must conclude that only minimal changes in the three-dimensional intrasubunit arrangement of PFn domains occur under acidic, alkaline, or high ionic strength conditions. Consequently, the Hörmann and Richter (1986) model, which predicts a critical role for the cleavage of intrasubunit electrostatic contacts during PFn assembly into multimeric fibrils, may require revision in light of this finding.

We have not elucidated the origin of the sensitivity of the ρ_H of PB-190/170 kDa to changes in pH. However, the following discussion by Weber (1953) provides the most likely explanation for this behavior: "It may be pointed out that small changes in molecular shape or volume are much more likely to be detected by a study of rotational diffusion than by sedimentation or translational diffusion. For a globular molecule the translational diffusion constant is roughly proportional to the cube root of the volume whereas the rotational relaxation time is proportional to the volume itself." However, it is not possible to exclude the possibility of pH-induced changes in the degree of PFn hydration contributing to this effect. There also exists the possibility that the intrasubunit salt bridges exhibit greater lability in the 190/170 kDa PFn fragment due to greater solvent accessibility. Since our present data support a structural model in which PFn and the 190/170-kDa PFn fragment display very similar intrasubunit (i.e., tertiary) structural characteristics, we consider this to be an unlikely possibility.

Rigid vs Flexible PFn Structures. A "flexible PFn structure" is usually defined as a structural configuration that permits the independent rotational and translational motion of each PFn domain. Assuming an average domain size of 30 kDa, flexible PFn structures would display ρ_H values on the 10^{-8} s time scale. Therefore, models that invoke extensive "flexibility" of the PFn peptide backbone (Williams et al., 1982; Lai & Tooney, 1984; Lai et al., 1984; Forastieri & Ingham, 1985; Ankel et al., 1986; Narasimhan & Lai, 1989) are incompatible with the slow (10^{-6} s) rotational relaxation times calculated from the PB-PFn and PB-190/170-kDa isothermal polarization data (Benecky et al., 1990; this study). On the basis of the above criteria, the structure of PFn is "rigid" at any given pH and/or ionic strength. If, however, one redefines PFn structural flexibility as a structure that permits the independent rotational motion of each PFn subunit, the structure of PFn is rigid under physiological buffer conditions and flexible under acidic, alkaline, or high ionic strength conditions.

Our present results question the validity of the correlation believed to exist between PFn structure under acidic, alkaline, and high ionic strength conditions and the appearance of PFn as a slender extended strand (140 nm × 2 nm) during electron-microscopic examination of rotary-shadowed PFn specimens (Engel et al., 1981; Erickson et al., 1981; Erickson & Carrell, 1983). In contrast, our results suggest that the unfolded PFn conformation can be approximated by a structure consisting of two disk-shaped subunits (each having an approximate diameter and thickness of 20 and 2.3 nm, respectively) that are each capable of independent rotational motion while remaining covalently linked to one another through the carboxy-terminal interchain disulfide bonds (model C in Scheme I). We believe that the extended structures observed during the electron-microscopic examination of rotary-shadowed specimens arise as a consequence of a conformational change triggered by PFn exposure to high glycerol concentrations during sample processing (Rocco et al., 1983).

Qualitatively, our model for the extended PFn conformation under acidic, alkaline, and high ionic strength conditions is compatible with the observed increase in the PFn radius of gyration under high ionic strength conditions (Rocco et al., 1987; Sjöberg et al., 1989) and the reported decrease in the PFn diffusion constant under alkaline conditions (Williams et al., 1982). This structural model is difficult to reconcile with the fluorescence energy transfer measurements of Lai and co-workers (Wolff & Lai, 1988, 1990), which indicate that 1 M NaCl has no effect on the PFn intersubunit distance. Clearly, further work is required to determine the origin of this discrepancy.

Recently, the rotational diffusion coefficient of bovine plasma fibronectin under physiological buffer conditions has been measured by electric birefringence (Vuillard et al., 1990). The rotational relaxation time reported in this study (0.76 μs) is significantly shorter than the ρ_H (4.4 μs) we previously obtained from fluorescence polarization measurements on PB-PFn under physiological buffer conditions (Benecky et al., 1990). However, the electric-birefringence-derived rotational relaxation time of bovine plasma fibronectin is similar in magnitude to the ρ_H values (1.05–1.23 μs) we presently obtain for PB-PFn in its unfolded conformation at pH 2, pH 11, or μ = 1.2 and pH 7.4 (this study). Since fibronectin is exposed to an applied electric field during the electric-birefringence measurement, we suggest that the applied field may cause bovine fibronectin to assume its unfolded conformation (i.e., model C in Scheme I) under the conditions of the electric-birefringence measurement.

Acknowledgments

We are grateful to Dr. John Fenton (New York State Dept. of Health, Albany, NY) for his generous gift of thrombin. We acknowledge the assistance provided by Dr. James Mattheis and John Catlo (SLM-Aminco, Inc., Urbana, IL) during the PB-PFn fluorescence lifetime measurements and Robert Ferguson (Marquette University Computer Science Division, Milwaukee, WI) during the quantitative analyses of the far-

ultraviolet CD data. We thank Angela Mallett for secretarial support.

References

Acuña, A. U., González-Rodriguez, J., Lillo, M. P., & Naqvi, K. R. (1987) *Biophys. Chem. 26*, 63–70.

Alexander, S. S., Colonna, G., & Edelhoch, H. (1979) *J. Biol. Chem. 253*, 1501–1505.

Ankel, E. G., Homandberg, G. A., Tooney, N. M., & Lai, C.-S. (1986) *Arch. Biochem. Biophys. 244*, 50–56.

Benecky, M. J., Kolvenbach, C. G., Amrani, D. L., & Mosesson, M. W. (1988) *Biochemistry 27*, 7565–7571.

Benecky, M. J., Kolvenbach, C. G., Wine, R. W., DiOrio, J. P., & Mosesson, M. W. (1990) *Biochemistry 29*, 3082–3091.

Brochon, J.-C., & Wahl, P. (1972) *Eur. J. Biochem. 25*, 20–32.

Cantor, C. R., & Schimmel, P. R. (1980) in *Biophysical Chemistry, Part II: Techniques for the Study of Biological Structure and Function*, pp 560–562, W. H. Freeman, New York.

Chen, A. B., Amrani, D. L., & Mosesson, M. W. (1977) *Biochim. Biophys. Acta 493*, 310–322.

Click, E. M., & Balian, G. (1985) *Biochemistry 24*, 6685–6696.

Engel, J., Odermatt, E., Engel, A., Madri, J., Furthmayr, H., Rohde, H., & Timpl, R. (1981) *J. Mol. Biol. 157*, 97–120.

Erickson, H. P. (1985) in *Plasma Fibronectin Structure and Function* (McDonagh, J., Ed.) pp 31–52, Marcel Dekker, New York.

Erickson, H. P., & Carrell, N. A. (1983) *J. Biol. Chem. 258*, 14539–14544.

Erickson, H., P., Carrell, N. A., & McDonagh, J. (1981) *J. Cell Biol. 91*, 673–678.

Forastieri, H., & Ingham, K. C. (1985) *J. Biol. Chem. 260*, 10546–10550.

Homandberg, G. A., & Erickson, J. W. (1986) *Biochemistry 25*, 6917–6925.

Homandberg, G. A., Amrani, D. L., Evans, D. B., Kane, C. M., Ankel, E., & Mosesson, M. W. (1985) *Arch. Biochem. Biophys. 238*, 652–663.

Hörmann, H., & Richter, H. (1986) *Biopolymers 25*, 947–958.

Knopp, J. A., & Weber, G. (1969) *J. Biol. Chem. 244*, 6309–6315.

Kornblihtt, A. R., Umezawa, K., Vibe-Pedersen, K., & Baralle, F. E. (1985) *EMBO J. 4*, 1755–1759.

Laemmli, U. K. (1970) *Nature (London) 22*, 680–685.

Lai, C.-S., & Tooney, N. M. (1984) *Arch. Biochem. Biophys. 228*, 465–473.

Lai, C.-S., Tooney, N. M., & Ankel, E. G. (1984) *Biochemistry 23*, 6393–6397.

Lakowicz, J. R. (1983a) *Principles of Fluorescence Spectroscopy*, pp 75–86, Plenum, New York.

Lakowicz, J. R. (1983b) *Principles of Fluorescence Spectroscopy*, pp 126–128, Plenum, New York.

Lakowicz, J. R. (1983c) *Principles of Fluorescence Spectroscopy*, pp. 260–271, Plenum, New York.

March, J. C., Parikh, I., & Cuatrecasas, P. (1974) *Anal. Biochem. 60*, 149–152.

Markovic, Z., Lustig, A., Engel, J., Richter, H., & Hörmann, H. (1983) *Hoppe-Seyler's Z. Physiol. Chem. 364*, 1795–1804.

Miekka, S. I., Ingham, K. C., & Menache, D. (1982) *Thromb. Res. 27*, 1–14.

Miller, G. L., & Golder, R. H. (1950) *Arch. Biochem. 29*, 420–423.

Mosesson, M. W., & Umfleet, R. A. (1970) *J. Biol. Chem. 245*, 5728–5736.

Mosesson, M. W., Chen, A. B., & Huseby, R. M. (1975) *Biochim. Biophys. Acta 386*, 509–524.

Narasimhan, C., & Lai, C.-S. (1989) *Biochemistry 28*, 5041–5046.

Odermatt, E., & Engel, J. (1989) in *Fibronectin* (Mosher, D. F., Ed.) pp 25–43, Academic Press, San Diego, CA.

Österlund, E. (1988) *Biochim. Biophys. Acta 955*, 330–336.

Österlund, E., Eronen, I., Österlund, K., & Vuento, M. (1985) *Biochemistry 24*, 2661–2667.

Perrin, F. (1934) *J. Phys. 5*, 497–511.

Petersen, T. E., Thøogersen, H. C., Skorstengaard, K., Vibe-Pedersen, K., Sahl, P., Sottrup-Jensen, L., & Magnusson, S. (1983) *Proc. Natl. Acad. Sci. U.S.A. 80*, 137–144.

Provencher, S. W., & Glöckner, J. (1981) *Biochemistry 20*, 33–37.

Rawitch, A. B., Hudson, E., & Weber, G. (1969) *J. Biol. Chem. 244*, 6543–6547.

Rocco, M., Carson, M., Hantgan, R., McDonagh, J., & Hermans, J. (1983) *J. Biol. Chem. 258*, 14545–14549.

Rocco, M., Infusini, E., Daga, M. G., Gogioso, L., & Cuniberti, C. (1987) *EMBO J. 6*, 2343–2349.

Sjöberg, B., Pap, S., Österlund, E., Österlund, K., Vuento, M., & Kjems, J. (1987) *Arch. Biochem. Biophys. 255*, 347–353.

Sjöberg, B., Eriksson, M., Österlund, E., Pap, S., & Österlund, K. (1989) *Eur. J. Biophys. 17*, 5–11.

Smith, R. L., & Griffin, C. A. (1985) *Thromb. Res. 37*, 91–101.

Sober, H. A., Ed. (1970) *CRC Handbook of Biochemistry*, 2nd ed., pp J288–J291, Chemical Rubber Co., Cleveland, OH.

Tooney, N. M., Mosesson, M. W., Amrani, D. L., Hainfeld, J. F., & Wall, J. S. (1983) *J. Cell Biol. 97*, 1686–1692.

Vuillard, L., Roux, B., & Miller, A. (1990) *Eur. J. Biochem. 191*, 333–336.

Wahl, P., & Weber, G. (1967) *J. Mol. Biol. 30*, 371–382.

Weber, G. (1952) *Biochem. J. 51*, 145–154.

Weber, G. (1953) *Adv. Protein Chem. 8*, 415–459.

Weber, G. (1981) *J. Phys. Chem. 85*, 949–953.

Weltman, J. K., & Edelman, G. M. (1967) *Biochemistry 6*, 1437–1447.

Williams, E. C., Janmey, P. A., Ferry, J. D., & Mosher, D. F. (1982) *J. Biol. Chem. 257*, 14973–14978.

Wolff, C., & Lai, C.-S. (1988) *Biochemistry 27*, 3483–3487.

Wolff, C., & Lai, C.-S. (1990) *Biochemistry 29*, 3354–3361.